

University of Groningen

Bimetallic Zeolite Beta Beads with Hierarchical Porosity as Brønsted-Lewis Solid Acid Catalysts for the Synthesis of Methyl Lactate

Pour, Zahra Asgar; Boer, Dina G.; Fang, Shun; Tang, Zhenchen; Pescarmona, Paolo P.

Published in:
Catalysts

DOI:
[10.3390/catal11111346](https://doi.org/10.3390/catal11111346)

IMPORTANT NOTE: You are advised to consult the publisher's version (publisher's PDF) if you wish to cite from it. Please check the document version below.

Document Version
Publisher's PDF, also known as Version of record

Publication date:
2021

[Link to publication in University of Groningen/UMCG research database](#)

Citation for published version (APA):

Pour, Z. A., Boer, D. G., Fang, S., Tang, Z., & Pescarmona, P. P. (2021). Bimetallic Zeolite Beta Beads with Hierarchical Porosity as Brønsted-Lewis Solid Acid Catalysts for the Synthesis of Methyl Lactate. *Catalysts*, 11(11), [1346]. <https://doi.org/10.3390/catal11111346>

Copyright

Other than for strictly personal use, it is not permitted to download or to forward/distribute the text or part of it without the consent of the author(s) and/or copyright holder(s), unless the work is under an open content license (like Creative Commons).

The publication may also be distributed here under the terms of Article 25fa of the Dutch Copyright Act, indicated by the "Taverne" license. More information can be found on the University of Groningen website: <https://www.rug.nl/library/open-access/self-archiving-pure/taverne-amendment>.





Take-down policy

If you believe that this document breaches copyright please contact us providing details, and we will remove access to the work immediately and investigate your claim.

Downloaded from the University of Groningen/UMCG research database (Pure): <http://www.rug.nl/research/portal>. For technical reasons the number of authors shown on this cover page is limited to 10 maximum.

Article

Bimetallic Zeolite Beta Beads with Hierarchical Porosity as Brønsted-Lewis Solid Acid Catalysts for the Synthesis of Methyl Lactate

Zahra Asgar Pour ¹, Dina G. Boer ^{1,2}, Shun Fang ¹, Zhenchen Tang ¹ and Paolo P. Pescarmona ^{1,*}

¹ Chemical Engineering Group, Engineering and Technology Institute Groningen (ENTEG), Faculty of Science and Engineering, University of Groningen, Nijenborgh 4, 9747 AG Groningen, The Netherlands; z.asgar.pour@rug.nl (Z.A.P.); d.g.boer@rug.nl (D.G.B.); s.fang@rug.nl (S.F.); z.tang@rug.nl (Z.T.)

² DMT Environmental Technology, Yndustrywei 3, 8501 SN Joure, The Netherlands

* Correspondence: p.p.pescarmona@rug.nl

Abstract: Bimetallic zeolite Beta in bead format and containing Al sites with Brønsted acid behavior and Sn, Zr or Hf sites with Lewis acid character, were prepared using a two-step synthetic route. First, zeolite Beta in the format of macroscopic beads (400 to 840 μm) with hierarchical porosity (micropores accessed through meso- and macropores in the range of 30 to 150 nm) were synthesized by hydrothermal crystallization in the presence of anion-exchange resin beads as hard template and further converted into their H-form. Next, the zeolite beads were partially dealuminated using different concentrations of HNO_3 (i.e., 1.8 or 7.2 M), followed by grafting with one of the above-mentioned metals (Sn, Zr or Hf) to introduce Lewis acid sites. These bimetallic zeolites were tested as heterogeneous catalysts in the conversion of dihydroxyacetone (DHA) to methyl lactate (ML). The Sn-containing zeolite Beta beads treated by 1.8 M HNO_3 and grafted with 27 mmol of SnCl_4 (Sn-deAl-1.8-Beta-B) demonstrated the best catalytic activity among the prepared bimetallic zeolite beads, with 99% selectivity and 90% yield of ML after 6 h at 90 °C. This catalyst was also tested in combination with Au-Pd nanoparticles supported on functionalized carbon nanotubes (CNTs) as multifunctional catalytic system for the conversion of glycerol to ML, achieving 29% conversion of glycerol and 67% selectivity towards ML after 4.5 h at 140 °C under 30 bar air. The catalytic results were rationalized by means of a thorough characterization of the zeolitic beads with a combination of techniques (XRD, N_2 -physisorption, SEM, XRF, TEM, UV-vis spectroscopy and pyridine-FT-IR).



Citation: Asgar Pour, Z.; Boer, D.G.; Fang, S.; Tang, Z.; Pescarmona, P.P. Bimetallic Zeolite Beta Beads with Hierarchical Porosity as Brønsted-Lewis Solid Acid Catalysts for the Synthesis of Methyl Lactate. *Catalysts* **2021**, *11*, 1346. <https://doi.org/10.3390/catal11111346>

Academic Editor: Jose L. Hueso

Received: 18 October 2021

Accepted: 5 November 2021

Published: 9 November 2021

Publisher's Note: MDPI stays neutral with regard to jurisdictional claims in published maps and institutional affiliations.



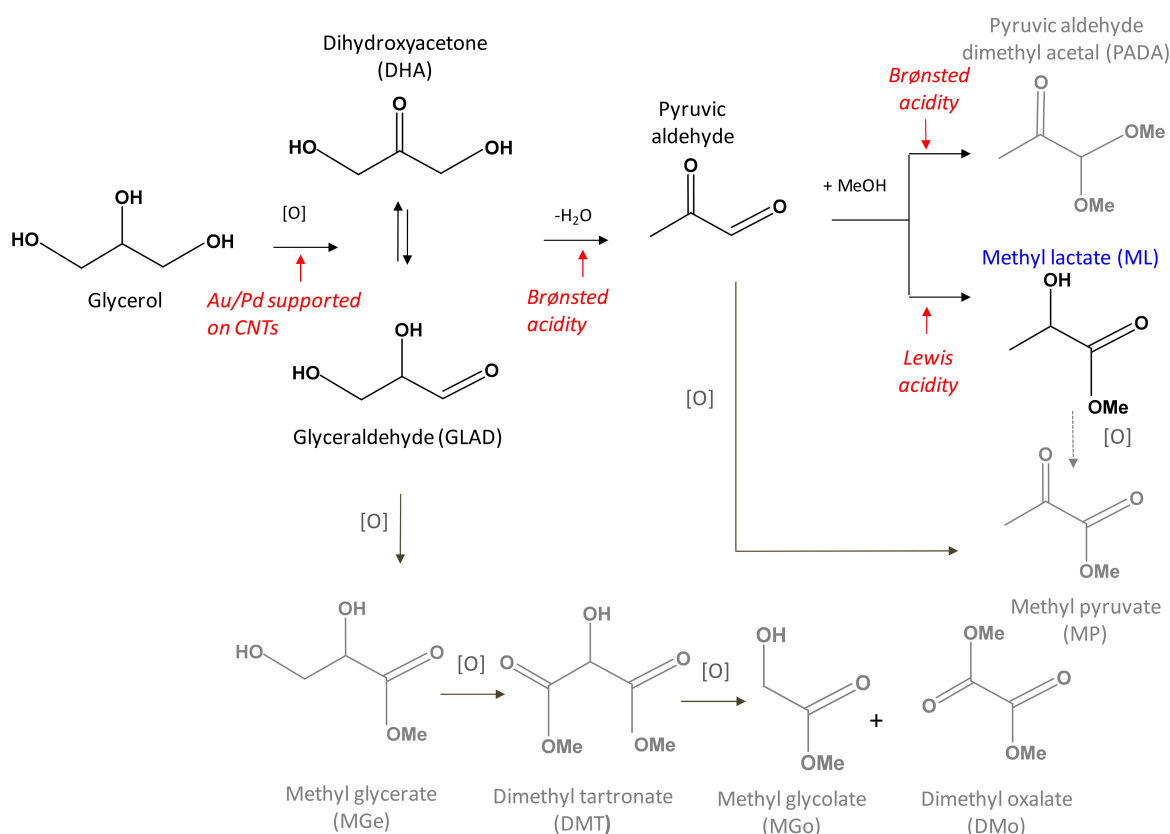
Copyright: © 2021 by the authors. Licensee MDPI, Basel, Switzerland. This article is an open access article distributed under the terms and conditions of the Creative Commons Attribution (CC BY) license (<https://creativecommons.org/licenses/by/4.0/>).

Keywords: methyl lactate; Sn-Al-Beta zeolite; hierarchical zeolites; Lewis acid zeolites; shaped catalysts; glycerol conversion

1. Introduction

The catalytic conversion of renewable feedstock into valuable chemicals is a key aspect of the transition towards a more sustainable chemical industry and has thus attracted growing attention from government, academia and companies in the past decades [1,2]. In particular, the depletion of fossil resources and global warming issues are two main driving forces for the increasing demand for the production of green, renewable biofuels [3,4]. In this context, the production of biodiesel from biobased triglycerides is a viable option and has shown a growing trend within the last decade [5], but it also implies that the glycerol generated as the main by-product of this process (10 wt%) should be upgraded to more applicable chemicals for preventing its oversupply in the market [6]. Partial oxidation of glycerol into trioses (i.e., 1,3-dihydroxyacetone (DHA) and glyceraldehyde (GLAD)) is an attractive catalytic route for the valorization of this compound. Further catalytic conversion of trioses in the presence of alcohols yields the biodegradable alkyl lactates (Scheme 1), which can be employed as green solvents with a wide range of applications [7]. Several catalysts have been reported for this last step, with heterogeneous ones being the preferred

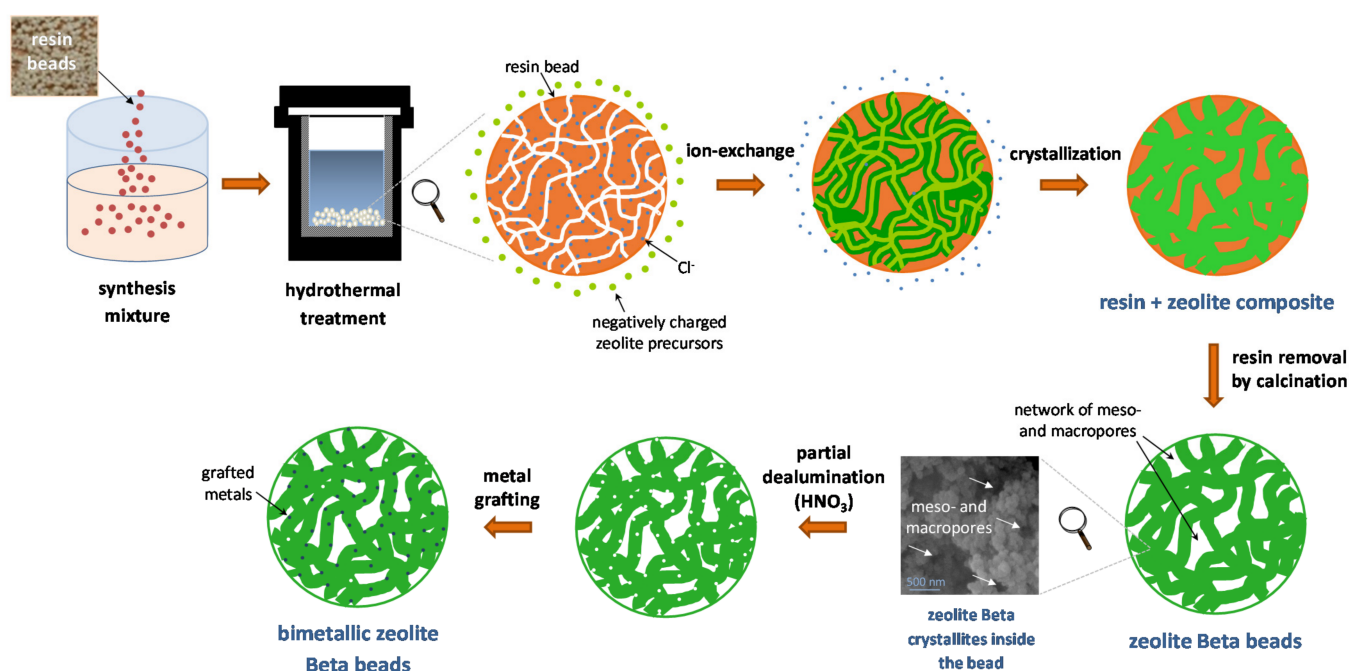
option in view of potential industrial application [8–10]. Typically, the heterogeneous catalysts displaying high activity and selectivity for this reaction contain (mild) Brønsted acid sites for catalyzing the dehydration of dihydroxyacetone or glyceraldehyde to the pyruvic aldehyde intermediate, and Lewis acid sites that promote the subsequent rearrangement with formation of methyl lactate (see Scheme 1) [7,11]. Particularly promising results were obtained with catalysts in which Sn atoms in tetrahedral coordination in a silicate matrix act as the Lewis acids sites, as in Sn-containing zeolites and ordered mesoporous silicates such as Sn-MCM-41 and Sn-SBA-15 [12–15]. If a suitable Sn-containing silicate is combined with a catalyst that is able to promote the dehydrogenative oxidation of glycerol to either dihydroxyacetone or glyceraldehyde, the one-pot conversion of glycerol to methyl lactate (Scheme 1) can be achieved. Indeed, supported metal nanoparticles (e.g., Au, Pd and alloys) have been employed in combination with nanosized Sn-MCM-41 to convert glycerol with high selectivity towards methyl lactate (87% selectivity at 81% glycerol conversion after 4.5 h reaction at 140 °C under 30 bar air) [7]. However, all the heterogeneous catalysts mentioned above were prepared and used in powder format. For industrial application, the use of catalyst powders is not practical and shaping into pellets is generally necessary. This is exemplified by fixed bed reactors, for which the use of powders can generate issues related to pressure drop. Pelletization does not come without disadvantages, as it typically requires the use of binders that allow the powders to be shaped into extrudates with good mechanical strength, but which also decrease the amount of active sites per gram of material and might negatively affect the surface area and the accessibility of the active sites [16,17].



Scheme 1. Catalytic route from glycerol to methyl lactate (ML) in the presence of methanol (in black). The possible by-products are shown in grey [7,14].

In this work, we aimed at combining the promising catalytic properties of Sn-containing zeolites for the conversion of trioses into lactates with structuring of these materials into binder-free macroscopic beads with hierarchical porosity. Avoiding the use of binders can allow overcoming the above-mentioned negative effects on the catalytic properties.

Our strategy to achieve binder-free shaping involved the use of macroscopic porous resin beads (Amberlite IRA 900 in Cl^- form with a size of 350 to 800 μm) as a hard template around which zeolite Beta crystals were formed by a tailored hydrothermal method. After removing the polymeric hard template by calcination, macroscopic beads were obtained, which contain microporous zeolite Beta crystals that are accessible through the meso- and macropores generated by removing the polymer (see Scheme 2). Such a hierarchical porous structure is expected to grant good accessibility to the zeolitic active sites [18–20], while the macroscopic bead format provides a binder-free shaping that facilitates the separation and recovery of the catalyst [21,22]. Next, the obtained beads were partially dealuminated by treatment with nitric acid, and Lewis acid metal centers (Sn, Zr or Hf) [23] were inserted by a grafting protocol [24]. This postsynthetic approach has been previously reported as a fluoride-free and thus safer and upscalable approach to prepare zeolites containing tunable amounts of Al and of a second metal (mostly Sn), thus combining Brønsted and Lewis acid sites [25–27].



Scheme 2. Synthesis method used to prepare bimetallic zeolite Beta beads.

All the prepared heterogeneous catalysts were tested in the synthesis of methyl lactate from dihydroxyacetone. The material that displayed the best catalytic performance was further applied in combination with Au-Pd supported on functionalized CNTs as heterogeneous catalytic system for the one-pot conversion of glycerol into methyl lactate. To the best of our knowledge, this is the first report of the synthesis of bimetallic, hierarchical and binder-free zeolite Beta beads possessing both Brønsted and Lewis acidity and of their application as heterogeneous catalysts for converting glycerol or its derivative dihydroxyacetone into methyl lactate.

2. Results and Discussion

A series of bimetallic and hierarchical zeolite Beta beads were synthesized using a tailored hydrothermal crystallization method followed by a post-synthetic treatment involving dealumination and metal-grafting steps. The parent zeolite Beta beads in H-form were prepared with a theoretical Si/Al = 13 using a hydrothermal synthesis method in the presence of Amberlite IRA 900 resin beads as hard template (see Section 3). The obtained material displayed the characteristic XRD pattern of zeolite Beta [BEA] (Figure 1, top) and high specific surface area (530 m^2/g). SEM analysis showed that the beads

have a diameter ranging from 400 to 850 μm (Figure 2A) and are characterized by a hierarchical internal structure in which interconnected zeolite particles form a network of meso- and macropores, mainly in the 30–150 nm range (Figure 2B and pore-size distribution based on N_2 physisorption in Figure S1B in the Supplementary Materials). The actual Si/Al determined by XRF analysis was 10 (Table 1). Besides the zeolite Beta beads, the procedure yielded zeolite Beta in conventional powder format as side product (see Figure S4 for the XRD pattern). Next, the prepared zeolite Beta beads sample was subjected to a treatment with different concentrations of nitric acid (1.8 or 7.2 M) to achieve different degrees of dealumination of the material [24]. The silanol groups generated through this dealumination step were utilized to graft Sn, Zr or Hf atoms, which were anticipated to act as Lewis acid sites [28].

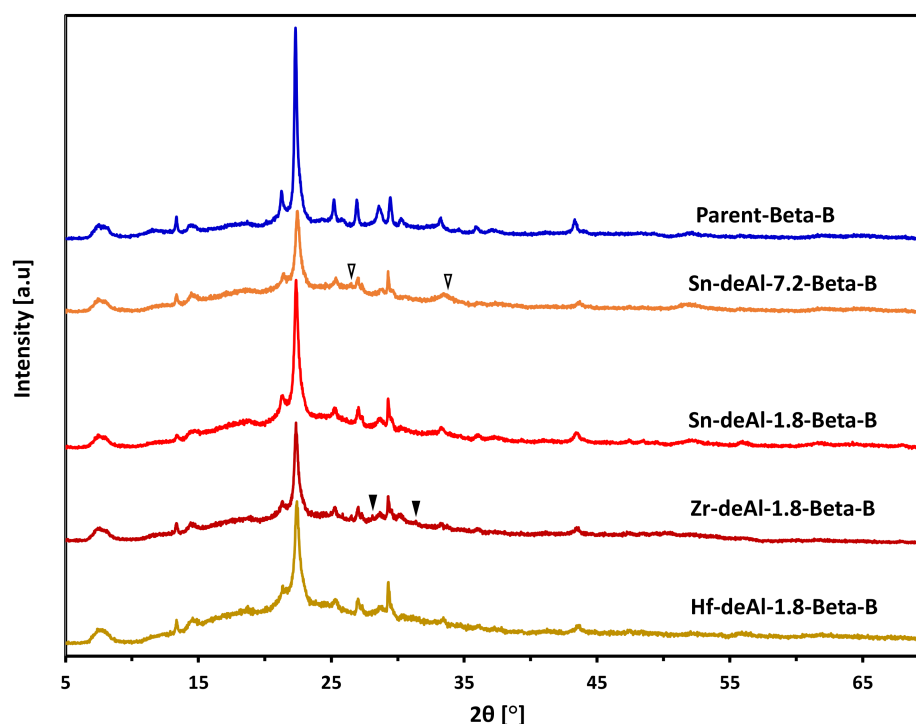


Figure 1. XRD patterns of the parent zeolite Beta beads and of the metal-containing Beta beads prepared by dealumination and following metal grafting; (▽) indicates signals from crystalline SnO_2 and (▼) indicates signals from crystalline ZrO_2 (magnified diffractograms highlighting the presence of these small amounts of metal oxides are provided in Figures S2 and S3).

Table 1. Physicochemical properties of the parent zeolite Beta beads and of the bimetallic zeolite Beta beads.

Entry	Catalyst	Specific Surface Area (m^2/g) ^a	$[\text{HNO}_3]$ for the Dealumination (M)	Si/Al Molar Ratio ^b	Si/Metal _{LA} Molar Ratio ^c
1	Parent zeolite Beta beads	530	-	10	-
2	Sn-deAl-1.8-Beta-B	442	1.8	40	50
3	Sn-deAl-7.2-Beta-B	432	7.2	80	133
4	Zr-deAl-1.8-Beta-B	355	1.8	32	13
5	Hf-deAl-1.8-Beta-B	339	1.8	28	55

^a BET surface area measured by N_2 physisorption. ^{b,c} Determined by XRF.

SEM analysis showed that in all cases the bead format and size was preserved after the acid treatment and the following grafting step (compare Figure 2C for Sn-Beta beads with Figure 2A for the parent Beta beads). The SEM images also indicate that the zeolite particles constituting the body of the beads and the structural meso- and macropores between them were not affected in a detectable way by the postsynthetic steps (compare

Figure 2B,D–G). This was confirmed by the unaltered pore-size distribution estimated from N_2 physisorption (Figure S1 in the Supplementary Materials).

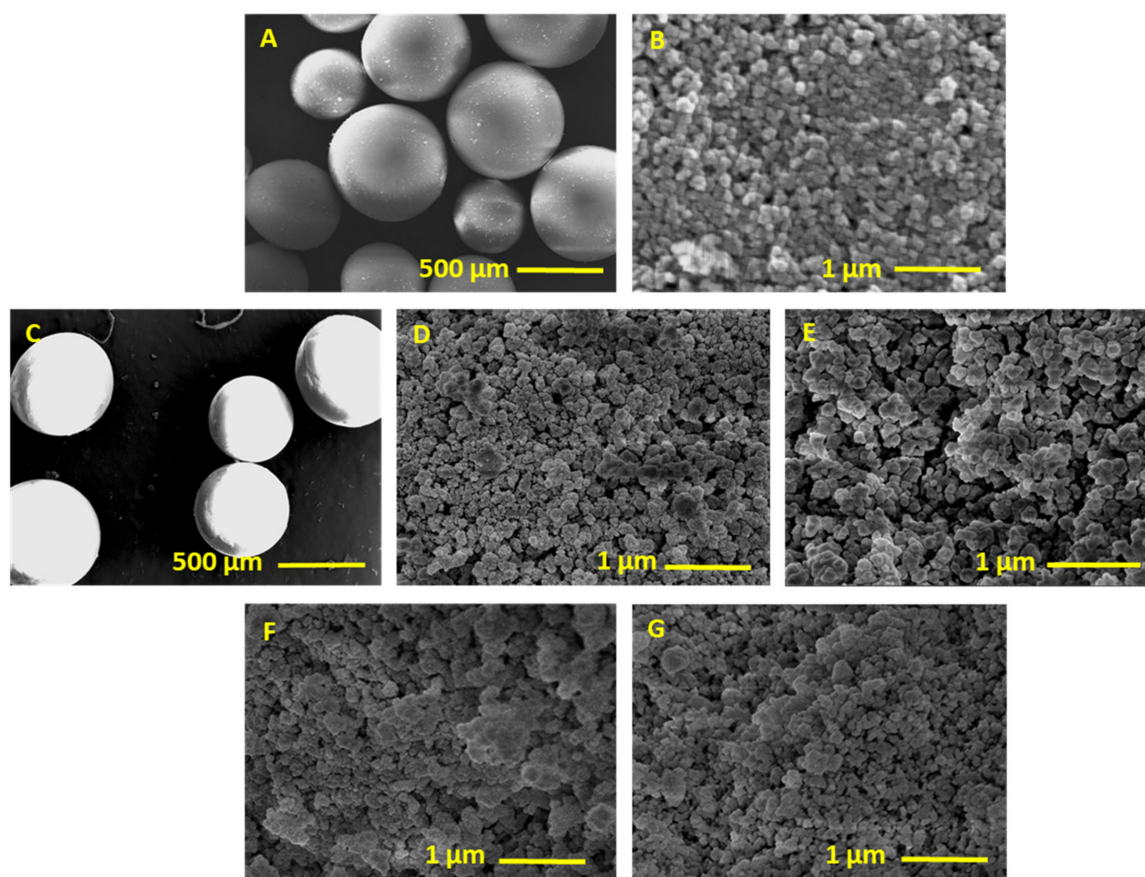


Figure 2. SEM images of (A) the parent zeolite Beta beads; (B) the surface morphology of the parent zeolite Beta beads; (C) Sn-deAl-1.8-Beta-B; (D) the surface morphology of Sn-deAl-1.8-Beta-B; (E) the surface morphology of Sn-deAl-7.2-Beta-B; (F) the surface morphology of Zr-deAl-1.8-Beta-B; and (G) the surface morphology of Hf-deAl-1.8-Beta-B.

XRD measurements of the Sn-containing beads (Figure 1) demonstrated that the crystalline structure of zeolite Beta was preserved after the acid treatment and the following grafting step. Additionally, minor traces of crystalline SnO_2 (see hollow triangle marker in Figure 1) might be present in Sn-deAl-7.2-Beta-B. The XRD pattern of Zr- and Hf-containing beads showed that also these materials retained the crystalline structure of zeolite Beta after the acid treatment and following metal grafting (Figure 1). Weak signals indicating the presence of a very small amount of crystalline ZrO_2 were observed in the Zr-containing beads (Figure 1, solid triangle markers). On the other hand, no extra signals were detected in the diffractogram of Hf-Beta beads, though this is more likely due to the amorphous nature of the HfO_2 species rather than to their absence (*vide infra*).

The degree of metal incorporation into the zeolite framework was investigated by means of diffuse reflectance UV-Vis spectroscopy. In the UV-Vis spectra of the two Sn-containing samples, the band at wavelength below 220 nm is assigned to isolated Sn species in tetrahedral coordination within the zeolitic framework (Figure 3A,B) [23,29]. The sample dealuminated with 7.2 M HNO_3 (Sn-deAl-7.2-Beta-B) displayed also a broad signal at about 235 nm, which has been ascribed to distorted tetrahedral or penta-coordinated framework Sn species and/or oligomeric extra-framework SnO_2 domains, and a second, partially overlapping broad band centered at 280 nm, which has been attributed to octahedrally-coordinated Sn in polymeric species such as bulk SnO_2 [29,30]. The same species are present in Sn-deAl-1.8-Beta-B, though the relative amount of the species giving the signal at

about 235 nm is significantly lower, leading to a single large band centered at about 270 nm in the UV-Vis spectrum. These results demonstrate that our materials contain the desired tetrahedral Sn species in the zeolite framework but also Sn sites with higher coordination that are expected to have less or no contribution to the catalytic activity, particularly in the case of the larger SnO₂ domains [29]. It should be noted that a similar variety of species is generally observed in Sn-Beta samples prepared by postsynthetic grafting [30]. The UV-Vis spectrum of the Zr-containing beads presents a band at wavelength below 220 nm and a second, partially overlapping band centered at about 230 nm (Figure 3C). The former signal is attributed to tetrahedrally coordinated Zr species whereas the latter is assigned to isolated Zr species but with distorted or higher coordination and/or to oligomeric ZrO₂ [23]. However, it should be noted that bulk ZrO₂ also has a maximum of absorption at about 230 nm, and a shoulder at around 300 nm [31], suggesting its presence in Zr-deAl-1.8-Beta-B. This is further supported by the small amount of bulk ZrO₂ domains identified by the XRD analysis (*vide supra*). Hf-containing beads also displayed a sharp peak at wavelength below 220 nm, which is attributed to isolated and tetrahedrally coordinated Hf (Figure 3D) [23]. In addition, the spectrum showed a broad band at around 235 nm and a shoulder at higher wavelengths that extended up to 330 nm, indicating the presence of Hf species with distorted or higher coordination [32]. Furthermore, it has been demonstrated that detection of bulk HfO₂ by UV-vis spectroscopy is challenging due to its weak absorption in the UV-vis range [23], implying that its formation cannot be excluded.

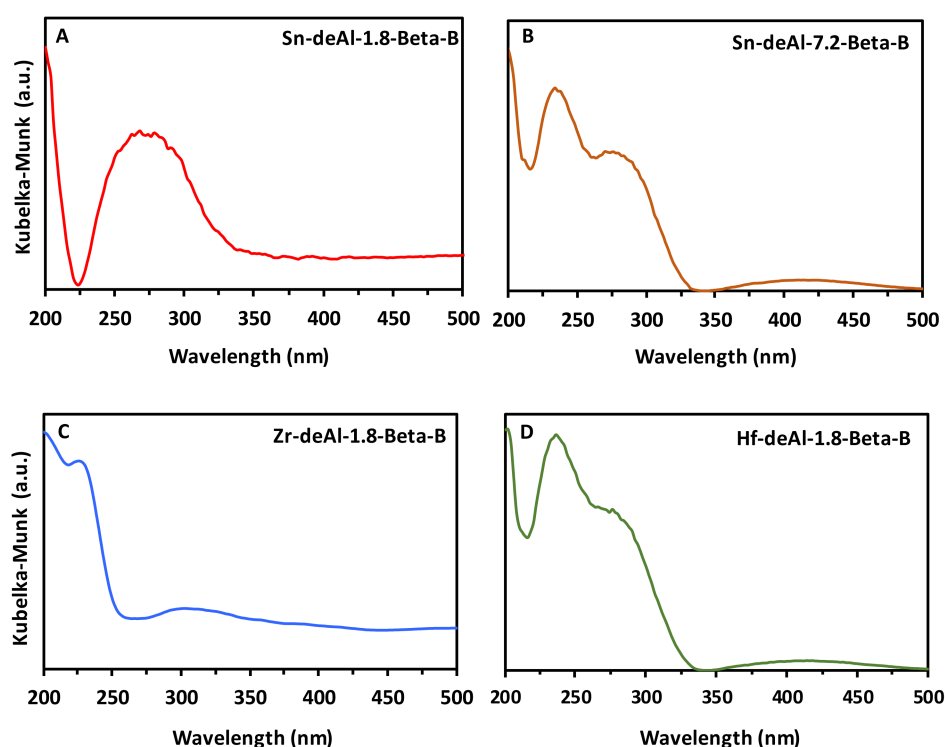


Figure 3. DR-UV-Vis spectra of metal-containing zeolite Beta beads after Kubelka–Munk correction: (A) Sn-deAl-1.8-Beta-B; (B) Sn-deAl-7.2-Beta-B; (C) Zr-deAl-1.8-Beta-B; (D) Hf-deAl-1.8-Beta-B.

XRF analysis demonstrated the expected higher Si/Al in the dealuminated samples compared to the parent zeolite Beta beads (Table 1). Additionally, an increase was observed in the amount of Al removed from the framework of the zeolites when increasing the HNO₃ concentration from 1.8 to 7.2 M in the dealumination step (Table 1, Entries 2 and 3), in line with logical expectations. The Sn-Beta beads dealuminated using 1.8 M HNO₃ also possessed higher amount of Sn in their structure compared to the counterpart prepared with 7.2 M HNO₃. In the Zr-containing zeolite beads, a remarkably high amount of Zr was observed by XRF analysis (Table 1, Entry 4), which suggests that this material also

contains a significant amount of extra-framework Zr species. The Hf-Beta beads showed approximately the same metal (IV) content as in Sn-Beta beads (Table 1, Entry 5), but a slightly higher Al content (similarly to Zr-Beta beads).

Analysis of the prepared materials by N₂ physisorption indicated that the postsynthetic treatments led to a decrease in specific surface area compared to the parent zeolite Beta beads (Table 1). This decrease is more significant for Zr- and Hf-containing beads (355 and 339 m²/g, respectively) than with the Sn-containing beads (442 and 432 m²/g). This trend is directly related to the increasingly higher atomic mass of Sn, Zr and Hf compared to Al, but might also be additionally caused by partial blocking of the pores of the beads due to the formation of oxide domains, as indicated by UV-Vis analysis. The N₂ physisorption isotherms of all the zeolite Beta beads are of IUPAC type IV (Figure S1 in the Supplementary Materials) with a steep increase in adsorption and a hysteresis loop at high p/p⁰ (> 0.9), in agreement with the presence of the network of connected meso- and macropores evidenced by SEM (*vide supra*) [33]. Coherently with this assignment, the isotherm of the zeolite Beta in powder form (Figure S1A) displays a much weaker increase in adsorption at p/p⁰ > 0.9, as this material does not contain the structural meso- and macropores that are characteristic of the bead samples.

The combination of the Lewis acidity introduced by grafting Sn, Zr or Hf and the Brønsted acidity stemming from Al atoms in tetrahedral sites in the zeolite framework is expected to be highly suitable for catalyzing the conversion of dihydroxyacetone to methyl lactate. Brønsted acidity catalyzes the triose dehydration step, whereas Lewis acidity catalyzes the rearrangement step of the intermediate pyruvic aldehyde into methyl lactate (Scheme 1) [7,24]. Based on these premises, the bimetallic zeolite beads were tested as heterogeneous catalysts in the conversion of dihydroxyacetone to methyl lactate under relatively mild conditions (90 °C, 6 h—see Table 2). The highest yields of methyl lactate were obtained with the Sn-Beta beads, which showed also high selectivity towards this product (Entries 1 and 2 in Table 2). The best catalytic performance was obtained with Sn-deAl-1.8-Beta-B, which reached 90% yield of methyl lactate with nearly full selectivity (99%) towards this compound. On the other hand, the Zr- and Hf-Beta beads displayed lower activity in the conversion of dihydroxyacetone into methyl lactate and yielded the dimethyl acetal of pyruvic aldehyde as main product (Entries 3 and 4 in Table 2). These results can be rationalized based on the features of the different catalysts evidenced by the physicochemical characterization discussed above. The highest activity of Sn-deAl-1.8-Beta-B compared to Sn-deAl-7.2-Beta-B is ascribed to the significant larger amount of Al and Sn sites in the former catalyst (see Si/Al and Si/Sn ratios in Table 1). This is reflected by the higher number of Brønsted and Lewis acid sites that was determined for Sn-deAl-1.8-Beta-B by FT-IR spectroscopic analysis of adsorbed pyridine (Figure 4 and Table 3). The lower Si/Al and thus higher Brønsted acid population in Sn-deAl-1.8-Beta-B are a consequence of the milder dealumination treatment. When comparing the number of Lewis acid sites per gram of material estimated by FT-IR of adsorbed pyridine with the number of Sn atoms per gram of material determined by XRF (304 μmol Sn/g for Sn-deAl-1.8-Beta-B and 120 μmol Sn/g for Sn-deAl-7.2-Beta-B), it follows that 20% of the Sn atoms in Sn-deAl-1.8-Beta-B act as Lewis acid sites, whereas the fraction is significantly higher in Sn-deAl-7.2-Beta-B (40%) [34]. This suggests that the Sn species that give the signal at 235 nm in the UV-Vis spectrum of Sn-deAl-7.2-Beta-B contribute to the Lewis acidity of the catalyst. This difference between the two Sn-Beta beads in the fraction of Sn atoms that behave as Lewis acid sites is reflected by the much higher turnover number (TON_{metal_{LA}}) observed with Sn-deAl-7.2-Beta-B, despite the lower methyl lactate yield (Table 2). The lower activity of Zr-deAl-1.8-Beta-B and Hf-deAl-1.8-Beta-B compared to their Sn-based counterpart (Sn-deAl-1.8-Beta-B) in the conversion of dihydroxyacetone can be ascribed to the observed lower specific surface area of the Zr- and Hf-containing catalysts. However, the most striking difference is the much higher yield and selectivity towards the dimethyl acetal of pyruvic aldehyde compared to the desired methyl lactate. It has been shown that this acetal product tends to form over catalysts in which the population of strong Brønsted

acid sites is predominant over the Lewis ones [11]. This suggests that the majority of Zr and Hf atoms in these materials are not acting as Lewis acid sites in the conversion of dihydroxyacetone to methyl lactate. XRF analysis showed that Zr-deAl-1.8-Beta-B and Hf-deAl-1.8-Beta-B have, respectively, higher or similar content of metal (IV) compared to Sn-deAl-1.8-Beta-B (Table 1) and the UV-Vis spectra suggest that a significant fraction of these metals is inserted in the zeolite framework and thus should behave as Lewis acid sites. The observed catalytic behavior cannot be ascribed either to the lower Lewis acid strength of these metal sites compared to their Sn counterparts [35,36], because Zr-TUD-1 and Hf-TUD-1 silicates with large, accessible mesopores have been reported to be active and selective heterogeneous catalysts for the title reaction [23]. Therefore, we propose that the Lewis acid sites in Zr-deAl-1.8-Beta-B and Hf-deAl-1.8-Beta-B are poorly accessible because of partial blockage of the micropores of the zeolite structure caused by metal oxide species and possibly also as a consequence of the larger ionic radius of Zr (IV) and Hf (IV) compared to Sn (IV), which decreases the space available in the micropores.

Table 2. Catalytic performance of Sn-, Zr- and Hf-containing zeolite Beta beads in the conversion of dihydroxyacetone (DHA) into methyl lactate (ML).

	Catalyst	Yield of ML (%)	Yield of PADA (%)	Selectivity (%)		TON _{metal,LA}
				ML	PADA	
1	Sn-deAl-1.8-Beta-B	90	0.4	99	1	57
2	Sn-deAl-7.2-Beta-B	76	6	92	8	120
3	Zr-deAl-1.8-Beta-B	10	53	16	84	2
4	Hf-deAl-1.8-Beta-B	9	23	28	72	6

Reaction conditions: 5 mL DHA 0.4 M in MeOH, 0.2 g of catalyst, 90 °C, 6 h. TON_{metal,LA} is defined as mol_{ML}/mol_{metal,LA}. ML: methyl lactate; PADA: pyruvic aldehyde dimethyl acetal.

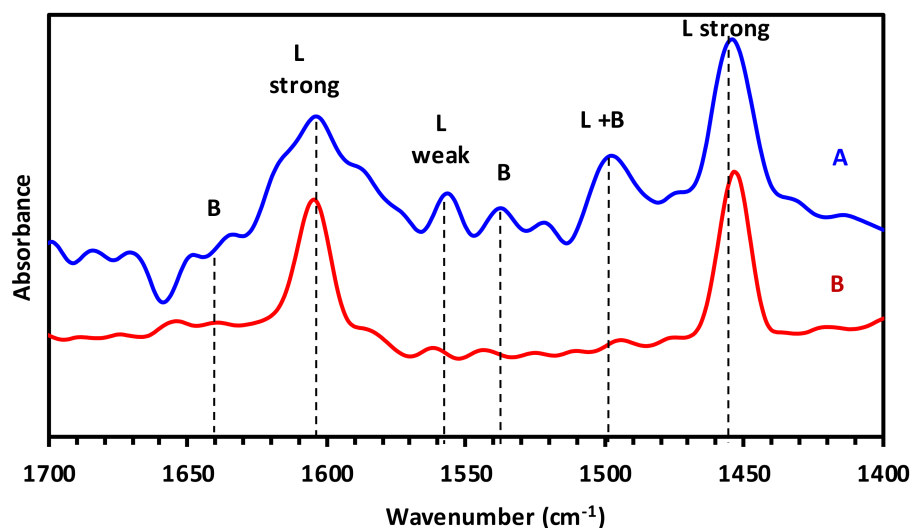


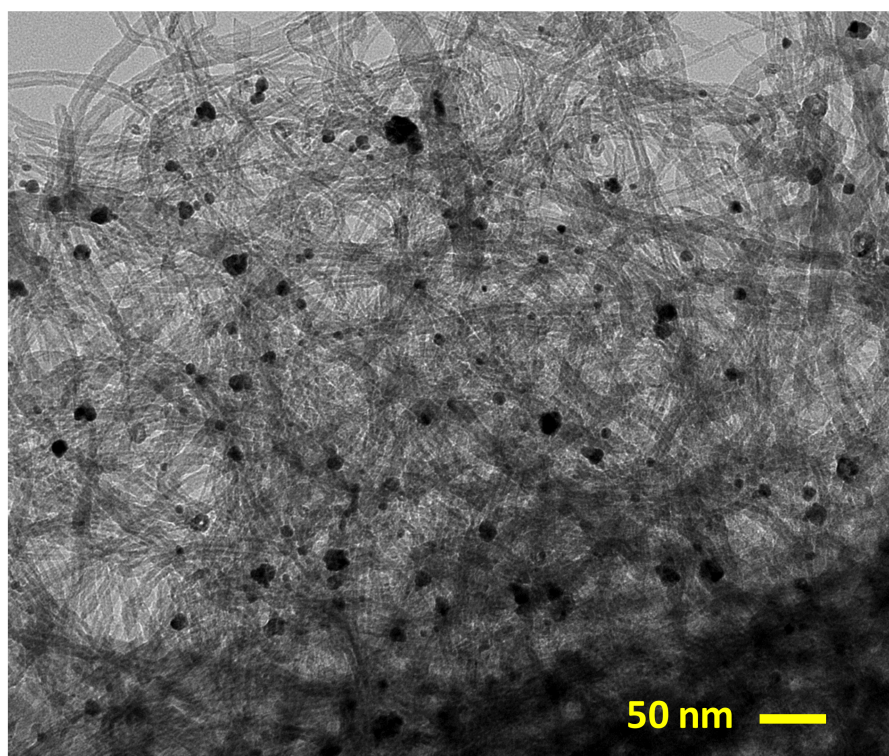
Figure 4. FT-IR spectra of pyridine adsorbed at 150 °C on A: Sn-deAl-1.8-Beta-B; B: Sn-deAl-7.2-Beta-B. L and B indicate peaks corresponding to Brønsted and Lewis acid sites, respectively. More specifically: the signals at 1450 and 1611 cm⁻¹ are ascribed to pyridine adsorbed on strong Lewis acid sites; the signal at 1560 cm⁻¹ is attributed to pyridine adsorbed on weak Lewis acid sites; the band centered at 1500 cm⁻¹ stems from both Brønsted and Lewis acid sites; the weak signals at 1540 and 1649 cm⁻¹ are assigned to protonated pyridine on Brønsted acid sites [26].

Table 3. Type and amount of surface acid sites in the Sn-Beta zeolite beads estimated by pyridine TPD-FT-IR.

Entry	Catalyst	Lewis Acid Sites ($\mu\text{mol/g}$)	Brønsted Acid Sites ($\mu\text{mol/g}$)	Lewis/Brønsted Ratio
		150 °C	150 °C	150 °C
1	Sn-deAl-1.8-Beta-B	60	13	5
2	Sn-deAl-7.2-Beta-B	48	3	16

The amounts of Lewis and Brønsted acid sites ($\mu\text{mol/g}$) were calculated from the integration of the bands at 1450 and 1500 cm^{-1} , respectively [37].

Based on the obtained results in the conversion of dihydroxyacetone to methyl lactate, Sn-deAl-1.8-Beta-B was identified as the most active catalyst among the investigated bimetallic zeolite Beta beads. The catalytic performance of this material is similar to that of state-of-the-art heterogeneous catalysts for the conversion of dihydroxyacetone into alkyl lactates [14,23,29,36,38], with the advantage of the bead format of the material, which allows its easy separation and recovery from the reaction mixture. To extend the scope of applicability of our optimum bead catalyst, Sn-deAl-1.8-Beta-B was tested in a physical mixture with Au-Pd nanoparticles supported on functionalized carbon nanotubes (AuPd-NP/CNT-F) as multifunctional catalytic system for the one-pot conversion of glycerol into methyl lactate. The Au-Pd nanoparticles supported on functionalized CNTs have been shown to be efficient in catalyzing the selective oxidation to a triose (dihydroxyacetone or glyceraldehyde) [7], which can then be converted into methyl lactate over the Sn-based catalyst. AuPd-NP/CNT-F with a total metal loading of 1 wt% was prepared according to a procedure recently reported by our group [7]. TEM analysis of the material showed the formation of well-dispersed nanoparticles on the carbon nanotubes (Figure 5). Most nanoparticles were found to have a size ≤ 5 nm, though some larger aggregates in the 10–25 nm range were also present.

**Figure 5.** TEM image of the Au-Pd nanoparticles supported on functionalized carbon nanotubes (AuPd-NP/CNT-F).

The heterogeneous catalytic system consisting of AuPd-NP/CNT-F and Sn-deAl-1.8-Beta-B was active in the conversion of glycerol to methyl lactate, though both product yield and selectivity were significantly lower compared to the state-of-the-art catalytic system for this reaction, in which nanosized Sn-MCM-41 particles in powder format are used instead of Sn-deAl-1.8-Beta-B (Table 4). Notably, the product distribution was rather different in the two cases. With the catalytic system consisting of AuPd-NP/CNT-F and Sn-deAl-1.8-Beta-B, the selectivity towards the desired methyl lactate product was lower (67%) and no methyl pyruvate (MP) was observed. On the other hand, higher selectivity was observed towards the methyl carboxylate products of the overoxidation of the glyceraldehyde intermediate, i.e., methyl glycerate (MGe), dimethyl tartronate (DMT), methyl glycolate (MGo), dimethyl oxalate (DMO) (Scheme 1). These results indicate that the cooperation between AuPd-NP/CNT-F and Sn-deAl-1.8-Beta-B is less efficient than in the literature optimum, because the trioses generated from the partial oxidation of glycerol over AuPd-NP/CNT-F are less readily converted into methyl lactate over Sn-deAl-1.8-Beta-B and instead are more likely to undergo further oxidation on the AuPd catalyst. This strongly suggests that the diffusion of the triose intermediates to the active sites of the macroscopic Sn-Beta zeolite beads is significantly slower compared to the diffusion to the highly accessible active sites of the nanosized Sn-MCM-41 particles (50–120 nm). A slower transfer would increase the probability that the triose intermediates are further oxidized over AuPd-NP/CNT-F rather than reaching the active sites of Sn-deAl-1.8-Beta-B to be converted into methyl lactate. The decreased proximity between the AuPd catalyst and the Sn-based catalyst also limits the transport of the formed methyl lactate from Sn-deAl-1.8-Beta-B to AuPd-NP/CNT-F, thus preventing its oxidation to methyl pyruvate (Scheme 1) and accounting for the absence of this normally observed by-product (Table 4). In our catalytic test we also observed the formation of 1,2-glycerol formal (GF), which is the product of the acetalization of formaldehyde—generated by partial oxidation of methanol—with glycerol. The higher selectivity towards this product compared to previous reports [7] is ascribed to the presence of strong acid sites in Sn-deAl-1.8-Beta-B, which are well-known to be active in catalyzing acetalization reactions [39,40].

Table 4. Catalytic performance of Sn-Beta zeolite beads in combination with AuPd-NP/CNT-F in the conversion of glycerol to methyl lactate.

Entry	Catalyst	Conv. (%)	Yield of ML (%)	Selectivity (%)						
				ML	MP	MGe	DMT	MGo	DMO	GF
1	Sn-deAl-1.8-Beta-B	29	20	67	n.d.	3.9	7.1	5.8	4.8	5.8
2	Sn-MCM-41-XS ^a	81	70	87	5.6	5.1	0.3	1.6	0.2	n.d.

Reaction conditions: 20 mL glycerol 0.25 M in MeOH, 0.1 g AuPd-NP/CNT-F, 0.2 g Sn-containing catalyst, 140 °C, 30 bar air, 4.5 h (n.d. = not detected). ^a Data taken from ref. [7].

3. Experimental Section

3.1. Materials

1,3-dihydroxyacetone dimer (97%), glycerol (99%), methyl glycolate (98%), methyl lactate (98%), tartronic acid (97%), dimethyl oxalate (99%), glyceric acid (20% in H₂O), methyl pyruvate (98%), tin chloride (SnCl₄, 98%), pyruvic aldehyde dimethyl acetal (98%), zirconium (IV) propoxide solution (Zr(OCH₂CH₂CH₃)₄, 70 wt% in 1-propanol), hafnium (IV) chloride (HfCl₄, 98%), tetraethyl orthosilicate (TEOS, 99%), tetraethylammonium hydroxide (TEAOH, 35 wt% in H₂O), Amberlite IRA 900 in Cl⁻ form, silica gel (high purity grade 9385), gold (III) chloride hydrate (AuCl₃, 99.999%), palladium (II) chloride (PdCl₂, 99.999%), polyvinyl alcohol (PVA, MW 9000–10,000, 80% hydrolyzed), sodium borohydride (99%), nitric acid (ACS reagent, 70 wt% HNO₃ in water) and multiwalled carbon nanotubes (CNTs > 95% purity, O.D. (outer diameter) × L (length) 6–9 nm × 5 μm were purchased from Sigma Aldrich (The Netherlands). Sulfuric acid (98%) was purchased from Merck (The Netherlands). Sodium aluminate anhydrous (purity 99.5%) was purchased from

Riedel-de Haën (Germany). MilliQ water was used for all steps of synthesis. No further pretreatment was applied for all-mentioned chemicals before using them in the synthesis of the catalysts and in the catalytic reactions.

3.2. Catalyst Synthesis

Zeolite Beta beads were synthesized by using Amberlite IRA 900 resin beads as hard templates and adapting an established hydrothermal method for the synthesis of zeolite Beta powder [41]. In a typical synthesis, 4.58 g of silica gel was partially dissolved in 17.71 g of tetraethylammonium hydroxide solution (TEAOH, 35 wt% in H₂O) and stirred for 1 h at room temperature. Next, an Al-containing solution was prepared by dissolving 0.57 g of NaAlO₂ in 10.74 g of H₂O under stirring for 10 min. This solution was added dropwise to the first mixture and further stirred for 1 h. Finally, the Amberlite IRA 900 resin beads were added to this mixture with a weight equal to one twentieth of the obtained suspension (1.68 g) [22]. This suspension was transferred into a 50 mL Teflon-lined autoclave, which was then closed and placed in an oven at 150 °C for 6 days in static condition. After this hydrothermal treatment, the autoclave was cooled down to room temperature, and opened. The obtained solids, consisting of zeolite Beta powder and beads with a typical bead-to-powder mass ratio of ca. 0.25, were separated from the liquid phase by filtration. Afterwards, the beads and powders were washed with H₂O (1 L) to reach pH around 7–8 and dried at 100 °C overnight. The beads were separated from the powder by sieving on a sieve with an aperture of 160 µm. Both beads and powder sample were calcined in a muffle furnace in static air with a two-step temperature program (3 °C/min from 20 °C to 200 °C, 6 h, 2 °C/min to 600 °C, 6 h) to remove the resin beads as spherical shaping template and the TEA⁺ as micropore structure directing agent. The obtained zeolites were in their Na-form. To convert them into their H-form, they were ion-exchanged using 1 M NH₄NO₃ aqueous solution (10 mL/g_{zeolite}) under stirring at 80 °C for 8 h. After the ion-exchange step, the samples were dried and calcined with the same calcination procedure mentioned above, thus yielding the H-form of zeolite, possessing Brønsted acidity. For embedding Lewis acid metals (Sn, Zr or Hf) into the zeolite structure, the parent zeolite beads were dealuminated using aqueous HNO₃ (1.8 M or 7.2 M, 55 mL/g_{zeolite}) under stirring at 80 °C for 15 h using a custom-made stirring vial with an overhead stirring rod (to prevent deterioration of the beads). Afterwards, the samples were filtered, washed to remove Al debris and dried at 60 °C overnight [24,42]. Next, the metal grafting step was carried out by adding 1 g of dealuminated zeolite to 100 mL of a 0.27 M solution of the appropriate metal precursor (i.e., 27 mmol of SnCl₄, Zr(OCH₂CH₂CH₃)₄ or HfCl₄) in dried 1-propanol, followed by stirring under N₂ blanketing and cooling water reflux for 7 h. Afterwards, each batch was filtered, washed with dry 2-propanol, dried at 60 °C and calcined with the temperature program described above. Dealuminated and metal grafted samples were labeled as M-deAl-c-Beta-B, in which “c” is the concentration of HNO₃ used in the dealumination step, “M” is the metal used in the grafting step, and “B” indicates the bead format.

The synthesis of Au-Pd nanoparticles supported on functionalized CNTs has been reported in previous work of our group [7]. Prior to use, the CNTs were treated and functionalized using nitric and sulfuric acid [7].

3.3. Characterization of the Catalysts

The crystallinity of the zeolite samples was investigated by X-ray diffraction (XRD) using a Bruker D-8 Advance-Germany diffractometer with Cu-K α radiation ($\lambda = 1.5418 \text{ \AA}$) generated at 40 kV and 40 mA. Data for the 2 θ angle were collected from 5 to 80° with a step size of 0.02° and a scan rate of 1°/min. The surface morphology was investigated by scanning electron microscopy (SEM) using a Philips XL30 ESEM FEG. Prior to SEM analysis, the zeolite samples were coated with a gold layer to make their surface conductive. The specific surface area of the prepared materials was measured by N₂ physisorption at −196 °C using a Micromeritics ASAP 2420. The BET (Brunauer-Emmet-Teller) and

BJH (Barret-Joyner-Halenda) models were applied to determine the specific surface area and pore size distribution, respectively. Prior to the N₂ physisorption, the samples were degassed at 300 °C for 12 h. The UV-Vis spectra were measured using a JASCO 570 UV–Vis-NIR absorption spectrometer with a scanning speed of 100 nm/min. Lewis and Brønsted acidity were measured by FT-IR spectroscopy using pyridine as a probe molecule in a Bruker Vertex 70 spectrometer equipped with a liquid nitrogen-cooled mercury-cadmium-telluride (MCT) detector with 4 cm⁻¹ resolution and 128 scans. The self-supported discs (approximately 30 mg, disc diameter ~ 1 cm) were pretreated at 400 °C under vacuum for 5 h to remove adsorbed water and then cooled down to room temperature. During the cooling step, the background spectra were recorded at 25 °C. Next, the samples were saturated with pyridine vapor at 20 mbar and 25 °C for 30 min and evacuated again for 30 min to remove the physisorbed pyridine. The evacuated samples were subjected to temperature-programmed desorption (TPD) at 150 °C for 30 min with a heating rate of 4 °C/min and the FT-IR spectra were recorded in situ at this temperature. The elemental analysis was performed with X-ray fluorescence (XRF) using a PANalytical Epsilon 3XLE equipment. 100 mg of the selected zeolite sample was analyzed and the amounts of each element (Si and the metal elements) were calculated assuming that these elements were in their oxide form. Transmission electron microscopy (TEM) images were taken using a CM12 (Philips) electron microscope working at 120 keV. The TEM samples were prepared by dispersion of the solid material in ethanol and sonication for 40 min. Next, one drop of prepared suspension was placed on a 400 mesh copper grid coated with carbon.

3.4. Catalytic Tests

The reaction of dihydroxyacetone (DHA) to methyl lactate (ML) in the presence of zeolite beads was conducted in a custom-made stirring vial equipped with an overhead stirring rod. This set-up allowed maintaining the shape integrity of the beads during the reaction. In a typical test, 5 mL of DHA solution (0.4 M in methanol) was added to 0.0215 g of *n*-decane as internal standard and heated at 45 °C for 30 min to convert the DHA dimer into the DHA monomer. Next, 0.2 g of zeolite catalyst was added to the reaction vial, followed by heating the reaction mixture to 90 °C for 6 h. Afterwards, the stirring and heating were turned off and the sample was allowed to cool down to room temperature. The beads settled at the bottom of the reaction vial upon stopping the overhead mechanical stirrer, thus not requiring any additional step for their separation from the reaction mixture. The products were quantified by injecting the reaction mixture into a GC (Thermo Tracer GC) equipped with a Restek Stabilwax-DA column (30 m length, 0.32 mm ID and 1 µm d_f) and a flame ionization detector (FID).

The yields of ML (main product) and of the pyruvic aldehyde dimethyl acetal (PADA) side product were calculated using Equations (1) and (2).

$$Y_{\text{ML}} = \frac{[\text{ML}]}{[\text{DHA}]_0} \times 100\% \quad (1)$$

$$Y_{\text{PADA}} = \frac{[\text{PADA}]}{[\text{DHA}]_0} \times 100\% \quad (2)$$

in which [ML] and [PADA] are the concentrations of the two products at the end of the reaction and [DHA]₀ is the initial DHA concentration. The selectivity towards ML and PADA was calculated by means of Equations (3) and (4):

$$S_{\text{ML}} = \frac{Y_{\text{ML}}}{Y_{\text{ML}} + Y_{\text{PADA}}} \times 100\% \quad (3)$$

$$S_{\text{PADA}} = \frac{Y_{\text{PADA}}}{Y_{\text{ML}} + Y_{\text{PADA}}} \times 100\% \quad (4)$$

Each compound was calibrated by four different concentrations. Due to its low response factor, the conversion of DHA cannot be measured by GC [11].

For the conversion of glycerol into ML, a 100 mL Parr stainless steel autoclave equipped with a Teflon liner was used. In a typical experiment, 20 mL glycerol (0.25 M in methanol) and a physical mixture of 0.1 g AuPd-NP/CNT-F and 0.2 g of Sn-containing zeolite beads were transferred into the reactor. Then, the mixture was stirred using an overhead mechanical stirrer at 800 rpm at 140 °C under 30 bar air pressure (oxidizing agent) for 4.5 h (0.5 h of heating time and 4.5 h at 140 °C, for a total of 5 h) [7]. At the end of the reaction, the autoclave was cooled down to ambient temperature and then depressurized. The catalyst was separated from the reaction solution by filtration and the liquid phase was tested using the above-mentioned GC. The conversion of glycerol was calculated using Equation (5):

$$\text{Conv.}_{\text{glycerol}} = \frac{[\text{gly}]_0 - [\text{gly}]}{[\text{gly}]_0} \times 100\% \quad (5)$$

in which $[\text{gly}]_0$ and $[\text{gly}]$ are the glycerol concentrations at the beginning and the end of the catalytic test, respectively. The selectivity of products was calculated by means of Equation (6):

$$S_P = \frac{[P]}{[\text{gly}]_0 - [\text{gly}]} \times 100\% \quad (6)$$

in which $[P]$ is the concentration of each product detected by GC. The carbon balance (C%) was calculated by summation of the amount of unreacted glycerol (as % of the initial amount) and the yields of products detected by GC.

All the catalytic tests for the conversion of dihydroxyacetone into methyl lactate were carried out in duplicate, showing $\pm 3\%$ reproducibility in the methyl lactate yield values. The reported yields were obtained by calculating the average of the two values obtained experimentally.

4. Conclusions

In this study, we developed several bimetallic zeolite Beta beads containing Lewis (Sn, Zr or Hf) and Brønsted (framework Al) acid sites by employing a two-step protocol. Firstly, zeolite Beta beads were synthesized by hydrothermal crystallization in the presence of anion-exchange resin beads as hard template. Next, the zeolite Beta beads were partially dealuminated by acid treatment and the sites from which Al was removed were employed to graft metal atoms with Lewis acid behavior (Sn, Zr or Hf). Among all metal-grafted catalysts, Sn-containing zeolites were highly active in the conversion of the glycerol-derived dihydroxyacetone into methyl lactate, reaching 90% yield and 99% selectivity after 6 h of reaction at 90 °C. This catalytic behavior is ascribed to the large population of Lewis and Brønsted acid sites that was evidenced by FT-IR spectroscopy of adsorbed pyridine, and to the hierarchical porosity and high specific surface area of the beads that were demonstrated by SEM and N_2 physisorption. This study showed that it is possible to produce binder-free bimetallic zeolite catalysts in the format of macroscopic beads and that high activity and selectivity in the conversion of dihydroxyacetone to methyl lactate can be achieved by carefully tuning the preparation method (i.e., the dealumination degree) and the nature of the Lewis acid metal. The optimum Sn-Beta beads were also tested in combination with Au-Pd nanoparticles supported on functionalized carbon nanotubes as multifunctional catalytic system for the one-pot conversion of glycerol to methyl lactate. The catalytic performance in this reaction was limited by the transport of the reaction intermediates between the two materials and achieved only moderate conversion of glycerol (29%) with 67% selectivity towards methyl lactate after 5 h at 140 °C under 30 bar air. Future work should aim at achieving proximity between the Au-Pd nanoparticles and the Sn and Al sites of the zeolite beads, which is expected to increase the yield and selectivity towards methyl lactate. Further future research directions can aim at exploiting the shaped binder-free nature of these zeolite beads in catalytic applications in fixed-bed reactors.

Supplementary Materials: The following are available online at <https://www.mdpi.com/article/10.3390/catal11111346/s1>, Figure S1: N_2 physisorption isotherms, Figure S2: Magnified X-ray

diffractograms of Sn-containing Beta beads and of commercial SnO₂, Figure S3: Magnified X-ray diffractograms of Zr-deAl-1.8-Beta-B and of commercial ZrO₂, Figure S4: X-ray diffractogram of the parent zeolite Beta powder.

Author Contributions: Conceptualization, P.P.P.; Data curation, Z.A.P., D.G.B., S.F. and P.P.P.; Formal analysis, Z.A.P. and P.P.P.; Funding acquisition, P.P.P.; Investigation, Z.A.P., D.G.B., S.F., Z.T. and P.P.P.; Methodology, Z.A.P., Z.T. and P.P.P.; Project administration, P.P.P.; Supervision, P.P.P.; Validation, Z.A.P. and P.P.P.; Visualization, Z.A.P.; Writing—original draft, Z.A.P.; Writing—review & editing, P.P.P. All authors have read and agreed to the published version of the manuscript.

Funding: We acknowledge funding for the Ph.D. project of Dina G. Boer by DMT Environmental Technology, Samenwerkingsverband Noord-Nederland (SNN) and GasTerra. We acknowledge the financial support from the China Scholarship Council (CSC) for the Ph.D. grants of S.F. and Z.T.

Data Availability Statement: The data are stored on the intranet of the University of Groningen (Y:\staff\se\Chemical Engineering) and are available upon request to the corresponding author.

Conflicts of Interest: The authors declare no conflict of interest.

References and Notes

1. Huber, G.W.; Iborra, S.; Corma, A. Synthesis of transportation fuels from biomass: Chemistry, catalysts, and engineering. *Chem. Rev.* **2006**, *106*, 4044–4098. [[CrossRef](#)]
2. Dapsens, P.Y.; Mondelli, C.; Pérez-Ramírez, J. Biobased chemicals from conception toward industrial reality: Lessons learned and to be learned. *ACS Catal.* **2012**, *2*, 1487–1499. [[CrossRef](#)]
3. Corma Canos, A.; Iborra, S.; Velty, A. Chemical routes for the transformation of biomass into chemicals. *Chem. Rev.* **2007**, *107*, 2411–2502. [[CrossRef](#)]
4. Sheldon, R.A. Green and sustainable manufacture of chemicals from biomass: State of the art. *Green Chem.* **2014**, *16*, 950–963. [[CrossRef](#)]
5. Mahlia, T.M.I.; Syazmi, Z.A.H.S.; Mofijur, M.; Abas, A.E.P.; Bilad, M.R.; Ong, H.C.; Silitonga, A.S. Patent landscape review on biodiesel production: Technology updates. *Renew. Sustain. Energy Rev.* **2020**, *118*, 109526. [[CrossRef](#)]
6. Alonso, D.M.; Wettstein, S.G.; Dumesic, J.A. Bimetallic catalysts for upgrading of biomass to fuels and chemicals. *Chem. Soc. Rev.* **2012**, *41*, 8075–8098. [[CrossRef](#)]
7. Tang, Z.; Boer, D.G.; Syariati, A.; Enache, M.; Rudolf, P.; Heeres, H.J.; Pescarmona, P.P. Base-free conversion of glycerol to methyl lactate using a multifunctional catalytic system consisting of Au-Pd nanoparticles on carbon nanotubes and Sn-MCM-41-XS. *Green Chem.* **2019**, *21*, 4115–4126. [[CrossRef](#)]
8. De Clippel, F.; Dusselier, M.; Van Rompaey, R.; Vanelderden, P.; Dijkmans, J.; Makshina, E.; Giebel, L.; Oswald, S.; Baron, G.V.; Denayer, J.F.M.; et al. Fast and selective sugar conversion to alkyl lactate and lactic acid with bifunctional carbon-silica catalysts. *J. Am. Chem. Soc.* **2012**, *134*, 10089–10101. [[CrossRef](#)]
9. Yamaguchi, S.; Yabushita, M.; Kim, M.; Hirayama, J.; Motokura, K.; Fukuoka, A.; Nakajima, K. Catalytic Conversion of Biomass-Derived Carbohydrates to Methyl Lactate by Acid-Base Bifunctional γ -Al₂O₃. *ACS Sustain. Chem. Eng.* **2018**, *6*, 8113–8117. [[CrossRef](#)]
10. West, R.M.; Holm, M.S.; Saravanamurugan, S.; Xiong, J.; Beversdorf, Z.; Taarning, E.; Christensen, C.H. Zeolite H-USY for the production of lactic acid and methyl lactate from C₃-sugars. *J. Catal.* **2010**, *269*, 122–130. [[CrossRef](#)]
11. Pescarmona, P.P.; Janssen, K.P.F.; Delaet, C.; Stroobants, C.; Houthoofd, K.; Philippaerts, A.; De Jonghe, C.; Paul, J.S.; Jacobs, P.A.; Sels, B.F. Zeolite-catalysed conversion of C₃ sugars to alkyl lactates. *Green Chem.* **2010**, *12*, 1083–1089. [[CrossRef](#)]
12. Osmundsen, C.M.; Spangsborg Holm, M.; Dahl, S.; Taarning, E. Tin-containing silicates: Structure-activity relations. *Proc. R. Soc. A Math. Phys. Eng. Sci.* **2012**, *468*, 2000–2016. [[CrossRef](#)]
13. Taarning, E.; Osmundsen, C.M.; Yang, X.; Voss, B.; Andersen, S.I.; Christensen, C.H. Zeolite-catalyzed biomass conversion to fuels and chemicals. *Energy Environ. Sci.* **2011**, *4*, 793–804. [[CrossRef](#)]
14. Tang, Z.; Fiorilli, S.L.; Heeres, H.J.; Pescarmona, P.P. Multifunctional Heterogeneous Catalysts for the Selective Conversion of Glycerol into Methyl Lactate. *ACS Sustain. Chem. Eng.* **2018**, *6*, 10923–10933. [[CrossRef](#)]
15. Pang, J.; Zheng, M.; Li, X.; Song, L.; Sun, R.; Sebastian, J.; Wang, A.; Wang, J.; Wang, X.; Zhang, T. Catalytic Conversion of Carbohydrates to Methyl Lactate Using Isolated Tin Sites in SBA-15. *ChemistrySelect* **2017**, *2*, 309–314. [[CrossRef](#)]
16. Jasra, R.V.; Tyagi, B.; Badheka, Y.M.; Choudary, V.N.; Bhat, T.S.G. Effect of clay binder on sorption and catalytic properties of zeolite pellets. *Ind. Eng. Chem. Res.* **2003**, *42*, 3263–3272. [[CrossRef](#)]
17. Michels, N.L.; Mitchell, S.; Pérez-Ramírez, J. Effects of binders on the performance of shaped hierarchical MFI zeolites in methanol-to-hydrocarbons. *ACS Catal.* **2014**, *4*, 2409–2417. [[CrossRef](#)]
18. Holm, M.S.; Taarning, E.; Egeblad, K.; Christensen, C.H. Catalysis with hierarchical zeolites. *Catal. Today* **2011**, *168*, 3–16. [[CrossRef](#)]
19. Pérez-Ramírez, J.; Christensen, C.H.; Egeblad, K.; Christensen, C.H.; Groen, J.C. Hierarchical zeolites: Enhanced utilisation of microporous crystals in catalysis by advances in materials design. *Chem. Soc. Rev.* **2008**, *37*, 2530–2542. [[CrossRef](#)] [[PubMed](#)]

20. Verboekend, D.; Mitchell, S.; Pérez-Ramírez, J. Hierarchical Zeolites Overcome all Obstacles: Next Stop Industrial Implementation. *Chim. Int. J. Chem.* **2013**, *67*, 327–332. [[CrossRef](#)] [[PubMed](#)]
21. Lin, K.; Li, L.; Sels, B.F.; Jacobs, P.A.; Pescarmona, P.P. Titanosilicate beads as versatile catalysts for the conversion of trioses to lactates and for the epoxidation of alkenes. *Catal. Today* **2011**, *173*, 89–94. [[CrossRef](#)]
22. Cheng, W.; Jiang, Y.; Xu, X.; Wang, Y.; Lin, K.; Pescarmona, P.P. Easily recoverable titanosilicate zeolite beads with hierarchical porosity: Preparation and application as oxidation catalysts. *J. Catal.* **2016**, *333*, 139–148. [[CrossRef](#)]
23. Li, L.; Cani, D.; Pescarmona, P.P. Metal-containing TUD-1 mesoporous silicates as versatile solid acid catalysts for the conversion of bio-based compounds into valuable chemicals. *Inorg. Chim. Acta* **2015**, *431*, 289–296. [[CrossRef](#)]
24. Dijkmans, J.; Dusselier, M.; Gabriëls, D.; Houthoofd, K.; Magusin, P.C.M.M.; Huang, S.; Pontikes, Y.; Trekels, M.; Vantomme, A.; Giebler, L.; et al. Cooperative catalysis for multistep biomass conversion with Sn/Al beta zeolite. *ACS Catal.* **2015**, *5*, 928–940. [[CrossRef](#)]
25. Tang, B.; Dai, W.; Wu, G.; Guan, N.; Li, L.; Hunger, M. Improved postsynthesis strategy to Sn-beta zeolites as lewis acid catalysts for the ring-opening hydration of epoxides. *ACS Catal.* **2014**, *4*, 2801–2810. [[CrossRef](#)]
26. Li, P.; Liu, G.; Wu, H.; Liu, Y.; Jiang, J.G.; Wu, P. Postsynthesis and selective oxidation properties of nanosized Sn-beta zeolite. *J. Phys. Chem. C* **2011**, *115*, 3663–3670. [[CrossRef](#)]
27. Wang, J.; Okumura, K.; Jaenicke, S.; Chuah, G.K. Post-synthesized zirconium-containing Beta zeolite in Meerwein-Ponndorf-Verley reduction: Pros and cons. *Appl. Catal. A Gen.* **2015**, *493*, 112–120. [[CrossRef](#)]
28. Dapsens, P.Y.; Mondelli, C.; Pérez-Ramírez, J. Design of Lewis-acid centres in zeolitic matrices for the conversion of renewables. *Chem. Soc. Rev.* **2015**, *44*, 7025–7043. [[CrossRef](#)]
29. Li, L.; Collard, X.; Bertrand, A.; Sels, B.F.; Pescarmona, P.P.; Aprile, C. Extra-small porous Sn-silicate nanoparticles as catalysts for the synthesis of lactates. *J. Catal.* **2014**, *314*, 56–65. [[CrossRef](#)]
30. Dijkmans, J.; Demol, J.; Houthoofd, K.; Huang, S.; Pontikes, Y.; Sels, B. Post-synthesis Sn β : An exploration of synthesis parameters and catalysis. *J. Catal.* **2015**, *330*, 545–557. [[CrossRef](#)]
31. Ramanathan, A.; Klomp, D.; Peters, J.A.; Hanefeld, U. Zr-TUD-1: A novel heterogeneous catalyst for the Meerwein-Ponndorf-Verley reaction. *J. Mol. Catal. A Chem.* **2006**, *260*, 62–69. [[CrossRef](#)]
32. Iida, T.; Ohara, K.; Román-Leshkov, Y.; Wakihara, T. Zeolites with isolated-framework and oligomeric-extraframework hafnium species characterized with pair distribution function analysis. *Phys. Chem. Chem. Phys.* **2018**, *20*, 7914–7919. [[CrossRef](#)]
33. Danumah, C.; Vaudreuil, S.; Bonneviot, L.; Bousmina, M.; Giasson, S.; Kaliaguine, S. Synthesis of macrostructured MCM-48 molecular sieves. *Microporous Mesoporous Mater.* **2001**, *44–45*, 241–247. [[CrossRef](#)]
34. Here, we are assuming that only Sn atoms act as Lewis acid sites. Extraframework Al species that might be present as residues of the dealumination process can also display Lewis acid character, but their contribution to the total Lewis acidity of the catalyst is expected to be minor and is thus omitted from this calculation.
35. Gunther, W.R.; Michaelis, V.K.; Griffin, R.G.; Roman-Leshkov, Y. Interrogating the lewis acidity of metal sites in beta zeolites with ¹⁵N pyridine adsorption coupled with MAS NMR spectroscopy. *J. Phys. Chem. C* **2016**, *120*, 28533–28544. [[CrossRef](#)]
36. Taarning, E.; Saravanamurugan, S.; Holm, M.S.; Xiong, J.; West, R.M.; Christensen, C.H. Zeolite-catalyzed isomerization of triose sugars. *ChemSusChem* **2009**, *2*, 625–627. [[CrossRef](#)]
37. Emeis, C.A. ChemInform Abstract: Determination of Integrated Molar Extinction Coefficients for IR Absorption Bands of Pyridine Adsorbed on Solid Acid Catalysts. *J. Catal.* **1993**, *141*, 347–354. [[CrossRef](#)]
38. Vivian, A.; Fusaro, L.; Debecker, D.P.; Aprile, C. Mesoporous Methyl-Functionalized Sn-Silicates Generated by the Aerosol Process for the Sustainable Production of Ethyl Lactate. *ACS Sustain. Chem. Eng.* **2018**, *6*, 14095–14103. [[CrossRef](#)]
39. Rodrigues, R.; Gonçalves, M.; Mandelli, D.; Pescarmona, P.P.; Carvalho, W.A. Solvent-free conversion of glycerol to solketal catalysed by activated carbons functionalised with acid groups. *Catal. Sci. Technol.* **2014**, *4*, 2293–2301. [[CrossRef](#)]
40. da Silva, C.X.A.; Gonçalves, V.L.C.; Mota, C.J.A. Water-tolerant zeolite catalyst for the acetalisation of glycerol. *Green Chem.* **2009**, *11*, 38–41. [[CrossRef](#)]
41. Wadlinger, R.L.; Kerr, G.T.; Rosinski, E.J. Catalytic Composition of a Crystalline Zeolite, Modil Oil Corporation. U.S. Patent 3,308,069, 7 March 1967.
42. Iglesias, J.; Moreno, J.; Morales, G.; Melero, J.A.; Juárez, P.; López-Granados, M.; Mariscal, R.; Martínez-Salazar, I. Sn-Al-USY for the valorization of glucose to methyl lactate: Switching from hydrolytic to retro-aldol activity by alkaline ion exchange. *Green Chem.* **2019**, *21*, 5876–5885. [[CrossRef](#)]